Unraveling Real-Time Dynamics in Mg-to-MgH_2 Phase Transformation Using In Situ Electron Microscopy

Gopi Krishnan,* Svetlana Korneychuk, Lars J. Bannenberg, Herman Schreuders, Joerg Jinschek, and Bernard Dam

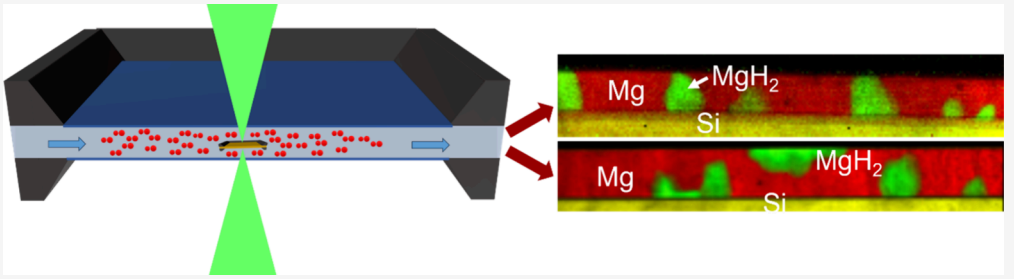

ABSTRACT: Using in situ scanning transmission electron microscopy (STEM) and low-loss plasmon electron energy-loss spectroscopy (EELS), we reveal asymmetric transformation mechanisms during the hydrogenation and dehydrogenation of Mg thin films. Remarkably, during hydrogenation, the MgH_2 phase can nucleate from either the bottom or top interface of a Mg thin film while symmetrically sandwiched between two Ti layers. This unexpected behavior, occurring under identical external conditions, highlights the critical role of nucleation barriers in the phase transformation process, challenging conventional diffusion-driven paradigms. In contrast, dehydrogenation proceeds exclusively via an H_2 diffusion-controlled frontal growth originating from the top interface. These insights underscore the importance of understanding metal-to-metal hydride phase transformations for advancing hydrogen storage technologies and applications such as hydrogen sensing.

In situ Mg to MgH_2 phase transformation in Mg thin films, where the MgH_2 transformation initiates at both the top and the bottom interface under the same conditions.

Understanding metal−hydrogen interactions and metal-to-metal hydride transformations is critical for advancing hydrogen-related technologies such as catalysis, energy storage and conversion, sensing, and mitigating hydrogen-induced material degradation.[1−9] Binary metal−hydrogen systems are fundamental models for studying these interactions, providing insights into phase transformations, diffusion mechanisms, and thermodynamic stability. Unraveling the transformation mechanism is crucial because it dictates how hydrogen is absorbed and released, influencing both the kinetics of phase transformation and the overall hydrogen storage capacity.[10] A key research question is whether the onset of the phase transformation is solely governed by the hydrogen diffusion gradient or involves an additional nucleation-and-growth process. To determine both these events requires high-resolution imaging and in situ observation to pinpoint precisely where and how the new phase emerges. Since the initial stages of phase transformation can be rapid, capturing these events in real-time is challenging. Here, we employ advanced in situ electron microscopy—specifically scanning transmission electron microscopy (STEM) and electron energy-loss spectroscopy (EELS)—to understand processes during the metal-to-metal hydride transformation.[11]

Magnesium (Mg) is widely regarded as an archetypal framework for exploring metal-hydride formation involving a solid−solid phase transformation and a change in point group symmetry.[10,12] In Mg thin films, with Pd as a catalyst to promote hydrogen dissociation and association, the phase transformation to magnesium hydride (MgH_2) is traditionally assumed and generalized to a hydrogen diffusion-controlled process and initiates at the Pd/Mg interface.[10,13−15] However, if MgH_2 formation were instead dominated by nucleation, the phase transformation could occur uniformly throughout the sample, assuming a homogeneous distribution of nucleation sites and a fast diffusion of hydrogen through the Mg metal.

Planar-view optical microscopy studies in samples with symmetric Mg interfaces (Pd/Ti/Mg/Ti films on Si substrates i.e., Mg is sandwiched between two Ti layers) indicated the

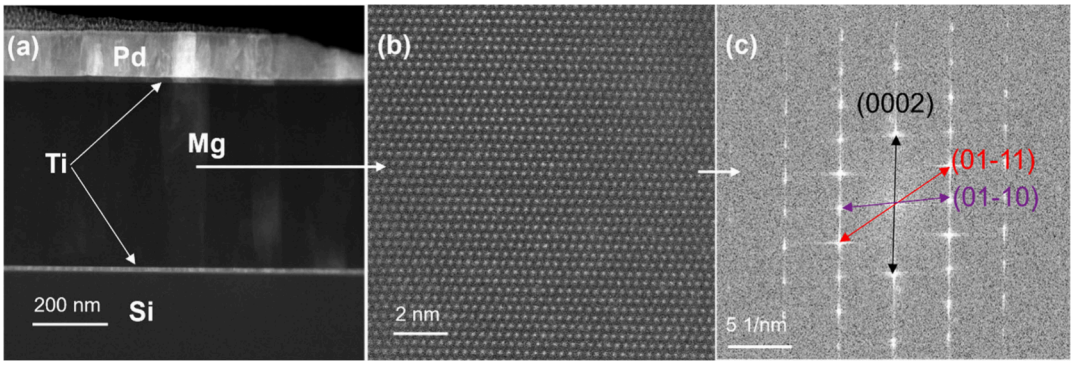

Figure 1. (a) HAADF STEM image of the FIB-prepared TEM lamella. (b) High-resolution STEM image of Mg from the region indicated by the arrow. (c) Fast Fourier transform of the HRSTEM shown in (b) in the [2−1−10] zone axis.

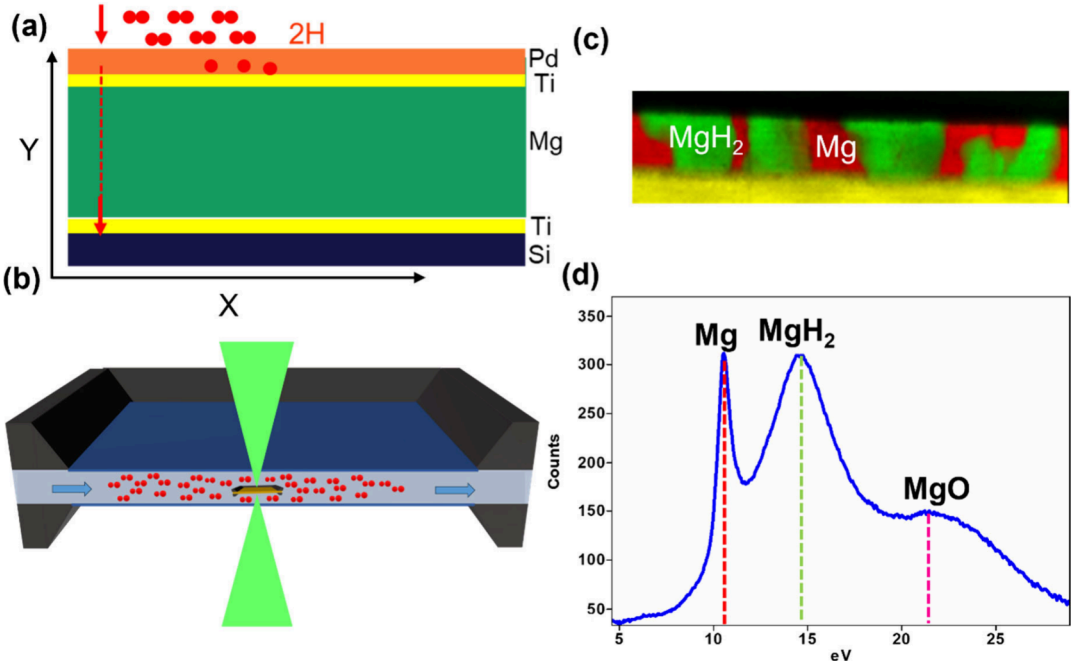

Figure 2. (a) Schematic of the cross-sectional view of the Mg lamella, where the H_2 enters from the top via Pd. (b) Schematic of the in situ gas cell setup with lamella. (c) Final snapshot of the Mg lamella during in situ hydrogenation of 200 mbar of H_2 at 75 °C. (d) EELS bulk plasmon resonance edges of Mg (10.4 eV), MgH_2 (14.5 eV), and MgO (22 eV) acquired at the in situ partial hydrogenation condition where both phases were present.

presence of nucleation and growth phenomena.[16−18] In these films, Mooij et al. observed lateral nucleation and growth of MgH_2 at hydrogenation pressures below 1 mbar.[16,17] In-situ neutron reflectometry indicated significant deviations from the thermodynamic solubility limits during the phase transformation in similar deuterated Mg thin film samples.[18] Note that during dehydrogenation, the Mg phase was observed to develop in a one-dimensional manner, suggesting a diffusion-controlled process and the absence of nucleation barriers.[16−19]

Cross-sectional studies on thin films using ex-situ and in situ electron microscopy indicate that MgH_2 growth originates from the top Pd/Mg interface in the form of nanocrystals.[20,21] However, given the sample's asymmetry in these studies (Mg is sandwiched between Pd and Si—Pd/Mg at the top, Mg/Si at the bottom-), it is unclear whether this is due to the H_2 diffusion gradient or to preferred nucleation at the top interface. The relevance of this behavior lies in the fact that the MgH_2 may severely hinder the hydrogenation of the underlying Mg due to the poor diffusion of hydrogen through MgH_2.[22]

Here, we use in situ STEM and EELS to investigate the (de)hydrogenation mechanism of Mg thin films having identical Mg/Ti top and bottom interfaces. This approach offers enhanced resolution and a wide field of view, enabling detailed visualization of the transformation dynamics. We monitor the cross-sectional phase transformation by tracking bulk plasmon shifts of Mg and MgH_2. Surprisingly, our results demonstrate that MgH_2 growth may be initiated both at the bottom and the top interface of the Mg film under identical conditions of hydrogen (H_2) pressures (200 mbar) and temperature (75 °C). Importantly, we did not observe any structural inhomogeneity at the interface that could account for the observed nucleation behavior. Our observation challenges the conventional assumption that hydrogenation is predominantly a diffusion-controlled transformation process. The fact that nucleation may start from the bottom interface offers new perspectives on the mechanisms driving (de)-

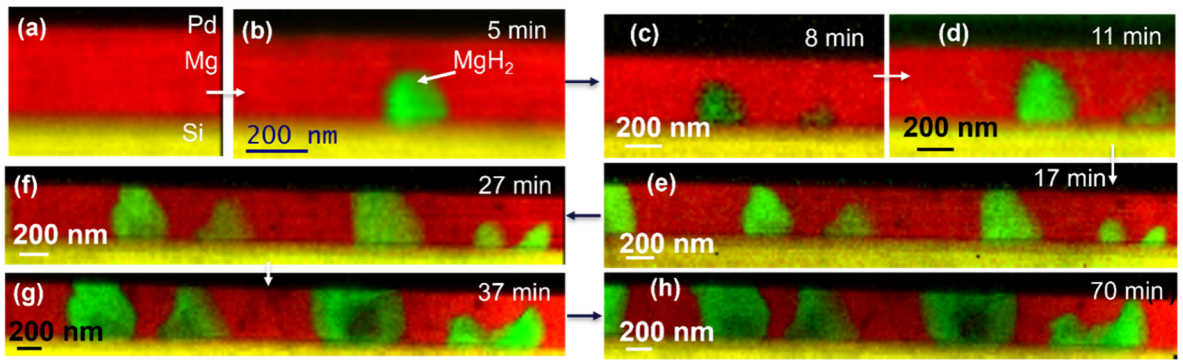

Figure 3. Nucleation and growth of MgH_2 during in situ hydrogenation at 75 °C and 200 mbar H_2, where nucleation of MgH_2 starts at the bottom Mg/Ti interface. (a)−(h) Progressive snapshots or MLLS maps of the phase transformation process taken at an interval during the hydrogenation process. Note that (c) shows the final snapshot of the transformed MgH_2. Each map is from the spectrum imaging EELS data set acquired at different stages.

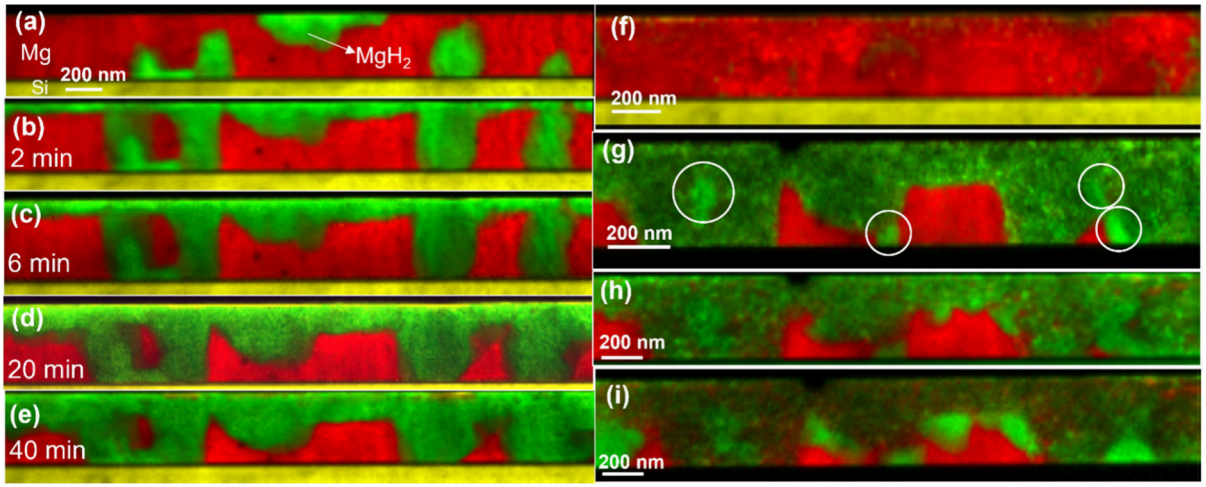

Figure 4. Mg to MgH_2 transformation via nucleation and growth and the H_2 diffusion-controlled mechanism simultaneously during in situ hydrogenation. Note: the top/bottom refers to the interface and not the figure panel. The transformation at the bottom interface represents nucleation and growth, and the transformation at the top represents the H_2 diffusion-controlled mechanism. (a)−(e) Snapshots or MLLS mapping of the first hydrogenation of the lamella: (b) after 2 min, (c) after 6 min, (d) after 20 min, and (e) final hydrogenation at 40 min, after which the hydrogenation becomes very slow or kinetically limited at 75 °C at 200 mbar. (f) E-beam-induced in situ dehydrogenated lamella. (g)−(i) Second hydrogenation of the same lamella at higher H_2 pressure. (g) Hydrogenation after 1 h at 75 °C at 270 mbar, with the circled region showing the hydrogenated area that was not hydrogenated in the first hydrogenation. (h), (i) Further hydrogenation snapshots at 20 and 40 min at 400 mbar. Each map is from the spectrum imaging of the EELS data set acquired at various stages of the transformation.

hydrogenation in Mg thin films and suggests strategies for designing more efficient materials for hydrogen storage and sensors. By controlling the precise nucleation and growth mechanisms, it may be possible to optimize hydrogen uptake and release, improving the overall performance of Mg and Mg-based materials in practical applications. Furthermore, this work highlights the broader utility of in situ STEM-EELS for studying processes in metal−hydrogen systems.

The Mg thin film stack is synthesized via DC magnetron sputtering, with the synthesis parameters presented in Figure S1 of the Supporting Information (SI).[23,24] The stack consists of a 400 nm thick Mg thin film grown on a Si substrate with a 100 nm thick Pd top layer to catalyze the dissociation and association of H_2 for (de)hydrogenation. An intermediate ∼ 12 nm Ti buffer layers are added to prevent alloying between Mg and Pd and/or between Mg and Si.[25] Mg is grown in (0002) orientation with columnar grain morphology, as indicated in the focused ion beam (FIB)-prepared cross-section lamella in Figure 1(a), also confirmed via X-ray diffraction (XRD) as shown in the SI.

The high-resolution STEM shown in Figure 1(b) also indicates the presence of (0002) orientation along the [2−1−10] zone axis, confirming the presence of Mg and its columnar growth.

The hydrogenation is performed at 200 mbar at 75 °C. Figure 2(a) presents a schematic of the Mg thin film in a cross-sectional view (akin to the FIB-prepared lamella), showing how hydrogen (H_2) enters the sample from the top through Pd. Before exposure, the lamella is attached to a MEMS microheater, shown in Figure S2 of the SI.

The sides of Mg and Ti are oxidized once the FIB lamella is exposed to open air during transfer to the TEM for analysis. The Mg at the lamella's sides oxidizes to a ∼2−5 nm thickness, forming an H_2 diffusion barrier. The energy barrier for H_2 dissociation on MgO is high, ranging from 2.3 to 3 eV, compared to Pd, which is less than 0.5 eV. Similarly, the TiO_2 that forms is also not an effective catalyst for hydrogen dissociation and hydrogenation, as it has a higher energy barrier (1.4 to 1.7 eV) than Pd. This allows H2 to diffuse only through Pd. The phase transformation of Mg to MgH_2 was

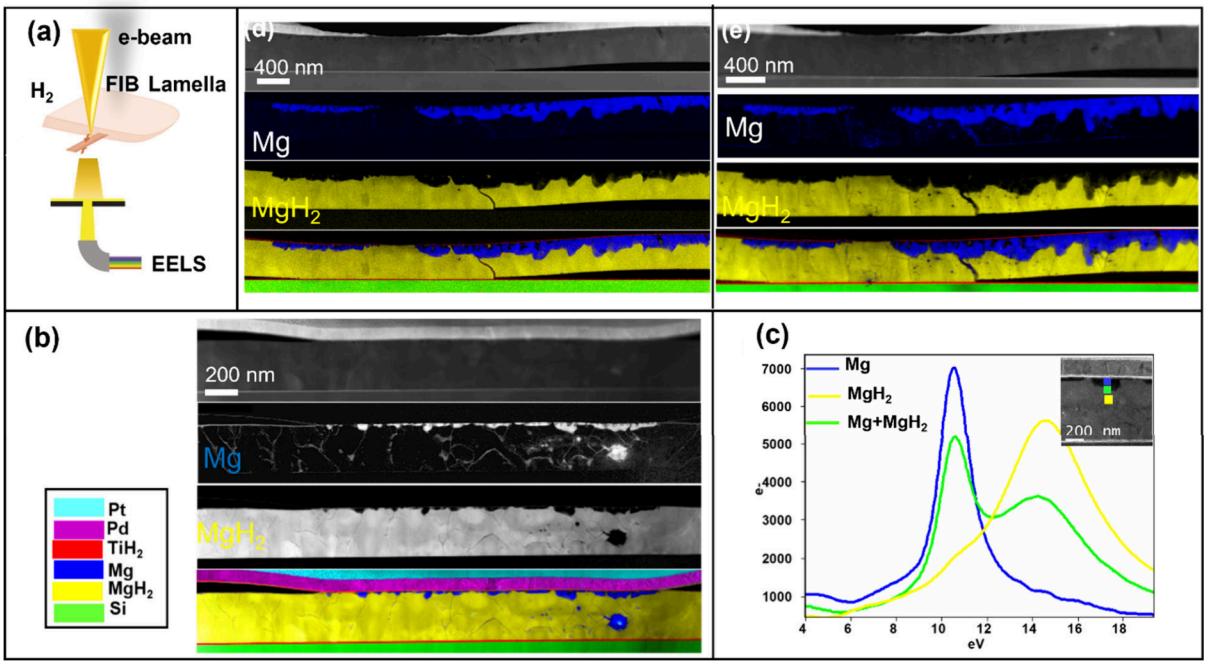

Figure 5. (a) Schematic of the e-beam-induced dehydrogenation of MgH_2. (b) A lamella in its inherent condition after it was completely hydrogenated ex situ and transported to TEM. In sequence from the top: HAADF STEM, Mg low-loss EELS map, MgH_2 low-loss EELS map, and a composite map of all the elements. (c) Low-loss EELS peaks at the top interface between Mg and MgH_2 and how the intermediate region displays both phases together. The inset also indicates the region where the low-loss peaks were collected. (d),(e) E-beam-induced dehydrogenation and their growth progress. The SI EELS data set of (e) was taken at a higher dose of electrons.

tracked via STEM-EELS by monitoring the bulk plasmon resonances of Mg (10.4 eV) and MgH_2 (14.5 eV) and a corresponding shift, as shown in Figure 2(d).[26] The corresponding multilinear least-squares (MLLS) mapping/fitting of individual phases is shown in Figure 2 (c) at the partial hydrogenation stage.

Figure 3 illustrates the nucleation and growth of MgH_2 during in situ hydrogenation via a gas cell/MEMS holder that allows studying phase transformation at higher pressures up to 1 bar of H_2.

Remarkably, the growth starts from the bottom Mg/Ti interface, away from the top Mg/Ti/Pd interface, from where the H_2 enters. It illustrates that, irrespective of H_2 diffusion gradient direction, nucleation may happen anywhere in the sample where the nucleation barrier is smallest and does not necessarily proceed from top to bottom, in contrast to what was reported for samples with an Mg/Pd interface.[20,21] It also indicates the possibility of substantial oversaturation of dissolved hydrogen in Mg.

Once the nucleation initiates at the bottom interface, it progresses both vertically and horizontally in the Mg film. Figure 3(a)−(h) represents snapshots of the phase transformation process acquired at different stages, preceding the snapshot shown in Figure 2(c). Each STEM-EELS spectrum imaging map of the different stages during phase transformation is taken at an interval of 10 to 15 min during the hydrogenation process. For each acquisition, the pressure was reduced to freeze the transformation to collect the growth of MgH_2. The electron beam dose rate and total dose used for the STEM-EELS mapping are given in Table S1 of the Supporting Information. As mentioned above, the fitting of the phases was done using MLLS, allowing the mapping of both phases simultaneously via bulk plasmon resonance shifts observed in low-loss EELS peaks (see the SI).

The in situ observation indicates that the vertical MgH_2 growth dominates initially, as the propagating front is toward the vertical direction. The lateral growth becomes more pronounced once the MgH_2-nanocrystal reaches the top Mg/Ti interface. We cannot unambiguously interpret the intensity gradient of the MgH_2 phase (green color) in the EELS MLLS mapping shown in Figure 3. It may indicate an overlap of MgH_x (α) and MgH_{2-y} (β) phases along the depth or electron beam direction, as shown in Figure S3 of the SI; alternatively, it suggests that the region is not entirely transformed to MgH_2 and displays substantial substoichiometry.

In a second experiment, another fresh FIB-lamella with similar lamella thickness (in electron beam direction) was hydrogenated under identical conditions. Figure 4 (a-e) shows the Mg-to-MgH_2 phase transformation at different stages of transformation.

In comparison to Figure 3, the initial kinetics of the transformation are faster. The images clearly show that MgH_2 formation occurs predominantly at the bottom. But, unlike the previous case, the Mg-to-MgH_2 transformation now also takes place at the top interface. After about 2 min, the top interface becomes fully covered with MgH_2 nuclei expanding downward, while growth proceeds from the bottom interface through a lateral expansion of the nuclei formed. However, the kinetics become very slow after 20 min of transformation, as shown in Figure 4(d),(e). The complete transformation is probably hindered by the slow diffusion of H in MgH_2 (diffusivity of H_2 in MgH_2 is 10^{-18} m^2 s^{-1}, 3 orders of magnitude lower than H_2 in Mg at 300 °C). Here, we are dealing with the so-called blocking effect, which is known to impair the hydrogenation kinetics of Mg.[27]

Since it is well-known that cycling may improve the hydrogenation kinetics, we investigated a second hydrogenation cycle of the lamella. In order to dehydrogenate the

sample, we used a 300 pA electron beam to scan the hydrogenated region (Figure 4(f)). In general, hydrogenation leads to the collapse of Mg columnar grain structure into a nanoparticulate structure, while dehydrogenation causes voids in the Mg thin films (Figures S4 and S5 in the SI).[16,17,21,28]

In the second hydrogenation cycle, we now observe an exceptionally rapid transformation,[16] making it experimentally challenging to pinpoint the exact nucleation sites or origin of the MgH_2 phase. The rapid transformation is probably due to the porous structure of the dehydrogenated film.[16] However, grains that were not hydrogenated during the first cycle do not easily transform into MgH_2. In fact, these areas only begin to hydrogenate at a higher H_2 pressure of 270−400 mbar. This transformation proceeds from both the bottom upward-(nucleation and growth) and downward from the top (H_2 diffusion-controlled), as shown in Figures 4(g)−(i). Apparently, certain grains seem to require higher pressures for hydrogenation, possibly due to a higher stress state requiring a higher overpotential.[29] A detailed investigation of grain orientation to confirm this hypothesis would provide further insights but lies beyond the scope of the present work.

In contrast to the nucleation- and growth-driven mechanism observed during hydrogenation, the formation of Mg by dehydrogenation follows a different pathway. Figure 5 shows the dehydrogenation process of the FIB lamella captured via in situ STEM-EELS, where dehydrogenation initiates at the top interface and progresses downward through the lamella.

The samples were first hydrogenated at 200 mbar H_2 and 75 °C, then transferred within a few minutes for STEM-EELS analysis. Figure 5(b) shows the EELS low-loss mapping of the initial dehydrogenation stage at the top Mg/Ti interface. This dehydrogenation was triggered by brief exposure to atmospheric conditions during lamella transfer. A low-dose electron beam was used to capture the dehydrogenation process in its pristine state and avoid e-beam-induced dehydrogenation, which is known to occur at higher electron doses.[26] The Mg region visible near the center of Figure 5(b) is attributed to prolonged electron-beam "parking" (i.e., unintentional beam exposure) in that area.

Figure 5(b),(d),(e) shows that voids and cracks form in the early stages of dehydrogenation. These voids, alongside Mg formation, appear at the top Mg/Ti interface to accommodate the 20−30% volume contraction in the Mg lattice.[19] The region around crack formation during phase transformation indicates Mg formation in the locality.[26] The voids tend to grow larger, and other voids start to appear as Mg grows. Once the sample is completely dehydrogenated, the voids cover all parts of the lamella, as shown in Figure S4 in Supporting Information. Remarkably, there is no measurable change in lamella height (y direction) postdehydrogenation.[19] Compared to the dehydrogenation shown in Figure 4(f), the initial voids at the interface in Figure 5(b) are due to lamella transfer rather than electron-beam-induced. Figure 5(c) shows bulk plasmon peaks for Mg and MgH_2, indicating a transition region where both phases coexist, similar to what was observed during in situ hydrogenation (Figures 3 and 4). Figure 5(d) illustrates one of the lamella windows experiencing dehydrogenation and Mg growth during lamella transfer under prolonged exposure to atmospheric conditions (note: 2−3 days in the air fully dehydrogenates the sample) and reveals Mg growth propagating from the top interface to the bottom. However, to observe the Mg propagation further in situ, a slightly higher electron dose was used to visualize Mg growth in real-time, as shown in Figure 5(e). Nevertheless, it is a controlled exposure and does not compromise the tracking of Mg growth.

When dehydrogenation is initiated by using a higher electron-beam dose in STEM, the dehydrogenation propagates from the top Mg/Pd interface toward the bottom, leading to complete phase transformations.[26] The Mg formation only initiates near the Pd interface as it provides a pathway for the release of hydrogen. Morover, Pd has the least energy to associate and dissociate H_2, as it equals <0.5 eV compared to 2.3 to 3.0 eV for MgO (which forms on the outer surface of the lamella during transfer to TEM.As shown in Figure 5(b), dehydrogenation only occurs when the Pd/Ti/Mg interface remains intact; otherwise, Mg formation is unfavorable. Therefore, Pd likely serves as a catalyst, with O_2 and H_2 reacting on the Pd surface to form water—a driving force for dehydrogenation under ambient conditions.[25,30] However, dehydrogenation does not show a transparent nucleation-based phase transformation process, unlike the hydrogenation process. Instead, we observe a 1D frontal growth front, which follows in the opposite direction of the hydrogen diffusion. This observation correlates well with previously reported in-plane thin film desorption studies, which also did not show any nucleation barriers.[16,17] Note: The dehydrogenation starts only from the top interface. Figure 5(b) shows pristine conditions without noticeable signs of e-beam-induced dehydrogenation.

The observed dehydrogenation process of MgH_2 can be explained as a H_2 diffusion-controlled growth process. It proceeds without a visible nucleation barrier, unlike in the case of hydrogenation. The reason for the absence of nucleation phenomena is likely to be due to the reduction in the volume on dehydrogenation. Therefore, compressive stresses do not play a role in the nucleation process.

In contrast to dehydrogenation, the volume expansion on hydrogenation is bound to influence the nucleation and growth behavior of MgH_2. However, our observations on the growth of MgH_2 differ from those reported by Hamm et al., who show nuclei starting from the top surface and first penetrating toward the bottom surface before expanding laterally.[21] They interpret this behavior as a consequence of local stress's development, which promotes nuclei's vertical expansion. It is unclear why we do not observe similar growth behavior. Even more remarkable are our observations of differences in nucleation. A thin film confined by the substrate should expand most easily at the top interface. At the same time, one must carefully consider the geometry of the FIB lamella and its constraints to compare them with the traditional thin film system in terms of the lamella's expansion during the MgH_2 phase transformation. We prepare the lamella thickness in the Z direction to be around 240 nm (thick) so that it is comparable to a thin film system.

However, nucleation at the bottom interface should induce markedly higher stresses and, therefore, require much higher supersaturations. It is unclear why we nevertheless observe this deviating behavior. To check for any difference that might favor or support the nucleation at one of the interfaces, we examined the morphology and structure of the bottom and top Mg/Ti interfaces at higher magnification. For instance, smaller grain sizes or random grain alignments in the initial stages of thin-film growth (before columnar growth is established) could promote bottom-interface nucleation, as reported for MgNi thin films transforming to Mg_2NiH_4.[31] However, we did not observe any inhomogeneities in the grain size. Note, however, that the stress distribution in asymmetric interfaces, such as

those presented by the experiments of Hamm et al., may differ from that in our symmetric interface, making it challenging to analyze the effects of such stresses on nucleation and growth.

Another difference with those experimental conditions is the fact that the MEMS-based microheaters used in these experiments were heated rapidly (instantaneously) to 75 °C, generating different stress levels at the top and bottom interfaces of the lamella. Since the bottom interface is bonded to a substrate, it experiences more strain during heating, as indicated by COMSOL simulation (Figure S6). This underscores the substantial influence that temperature changes can exert on the hydrogenation mechanism, even when overall external heating conditions appear consistent. Thus, whichever interface—top or bottom—offers the lower energy barrier for MgH_2 nucleation will determine where the Mg hydride nucleation and transformation begin.[31]

Summarizing, in situ STEM-EELS reveals that in Mg thin films with a symmetric interface, a nucleation-driven mechanism for MgH_2 formation may originate at the bottom interface, opposite the top interface where hydrogen enters. It contrasts with the conventional assumption that the nucleation of MgH_2 predominantly follows the diffusion gradient and shows that a substantial oversaturation may occur within the Mg lamella. In the case that nucleation starts from the top surface, it proves to be difficult to fully hydrogenate the sample. Our results show that this well-known blocking effect may thus also be circumvented by introducing sufficient nucleation centers within an Mg sample. The reason for the preferred nucleation at the bottom interface in our samples may relate to inhomogeneities and thermally induced stresses. Conversely, dehydrogenation invariably proceeds via a frontal growth mechanism, starting at the top interface and advancing downward toward the bottom interface, showing an asymmetry between hydrogenation and dehydrogenation. This study provides novel insights into phase transformation dynamics and underscores the broader applicability of in situ STEM-EELS for exploring metal−hydrogen systems.

AUTHOR INFORMATION

Corresponding Author

Gopi Krishnan − *National Centre of Nano Fabrication and Characterization, DTU Nanolab, Technical University of Denmark, Kongens Lyngby 2800, Denmark;* orcid.org/0000-0002-9932-2805; Email: Gopikrishnan1145@gmail.com

Authors

Svetlana Korneychuk − *Karlsruhe Nano Micro Facility (KNMFi), Karlsruhe Institute of Technology (KIT), 76344 Eggenstein-Leopoldshafen, Germany; Institute for Applied Materials − Materials Science and Engineering (IAM-WK), Karlsruhe Institute of Technology, 76131 Karlsruhe, Germany; Institute of Nanotechnology, Karlsruhe Institute of Technology, 76344 Eggenstein-Leopoldshafen, Germany*

Lars J. Bannenberg − *Faculty of Applied Sciences, Delft University of Technology, Delft 2629JB, The Netherlands;* orcid.org/0000-0001-8150-3694

Herman Schreuders − *Faculty of Applied Sciences, Delft University of Technology, Delft 2629JB, The Netherlands*

Joerg Jinschek − *National Centre of Nano Fabrication and Characterization, DTU Nanolab, Technical University of Denmark, Kongens Lyngby 2800, Denmark;* orcid.org/0000-0003-1574-0899

Bernard Dam − *Faculty of Applied Sciences, Delft University of Technology, Delft 2629JB, The Netherlands;* orcid.org/0000-0002-8584-7336

Notes

The authors declare no competing financial interest.

ACKNOWLEDGMENTS

This project has received funding from the European Union's Horizon 2020 research and innovation programme under the Marie Skłodowska-Curie grant agreement No 101028381. This work was partly carried out with the support of the Karlsruhe Nano Micro Facility (KNMFi, www.knmf.kit.edu), a Helmholtz Research Infrastructure at Karlsruhe Institute of Technology (KIT, www.kit.edu). We thank Dr. Murat Yesibolati and Prof. Christian Damsgaard for their help. Prof. Jakob Wagner is acknowledged for an interesting discussion and input on the results. G.K. also thanks Prof. Christian Kubel and Dr. Di Wang for hosting a Marie-Curie Fellowship secondment at KIT for the in situ experiment and for their support throughout the visit.

REFERENCES

(1) Klopčič, N.; Grimmer, I.; Winkler, F.; Sartory, M.; Trattner, A. A Review on Metal Hydride Materials for Hydrogen Storage. *Journal of Energy Storage* **2023**, *72*, 108456.

(2) Yu, H.; Li, X.; Zheng, J. Beyond Hydrogen Storage: Metal Hydrides for Catalysis. *ACS Catal.* **2024**, *14* (5), 3139.

(3) Wang, Q.; Guo, J.; Chen, P. Complex Transition Metal Hydrides for Heterogeneous Catalysis. *Chem. Catalysis* **2023**, *3*, 100524.

(4) Haddad, A. Z.; Garabato, B. D.; Kozlowski, P. M.; Buchanan, R. M.; Grapperhaus, C. A. Beyond Metal-Hydrides: Non-Transition-Metal and Metal-Free Ligand-Centered Electrocatalytic Hydrogen Evolution and Hydrogen Oxidation. *J. Am. Chem. Soc.* **2016**, *138*, 7844.

(5) Møller, K. T.; Sargent, A. L.; Remhof, A.; Heere, M. Beyond Hydrogen Storage—Metal Hydrides as Multifunctional Materials for Energy Storage and Conversion. *Inorganics* **2020**, *8*, 58.

(6) Nugroho, F. A. A.; Darmadi, I.; Cusinato, L.; Susarrey-Arce, A.; Schreuders, H.; Bannenberg, L. J.; da Silva Fanta, A. B.; Kadkhodazadeh, S.; Wagner, J. B.; Antosiewicz, T. J.; Hellman, A.; Zhdanov, V. P.; Dam, B.; Langhammer, C. Metal−Polymer Hybrid Nanomaterials for Plasmonic Ultrafast Hydrogen Detection. *Nat. Mater.* **2019**, *18* (5), 489.

(7) Wadell, C.; Syrenova, S.; Langhammer, C. Plasmonic Hydrogen Sensing with Nanostructured Metal Hydrides. *ACS Nano* **2014**, *8*, 11925.

(8) Bannenberg, L. J.; Boelsma, C.; Asano, K.; Schreuders, H.; Dam, B. Metal Hydride Based Optical Hydrogen Sensors. *J. Phys. Soc. Jpn.* **2020**, *89*, 051003.

(9) Yu, H.; Díaz, A.; Lu, X.; Sun, B.; Ding, Y.; Koyama, M.; He, J.; Zhou, X.; Oudriss, A.; Feaugas, X.; Zhang, Z. Hydrogen Embrittlement as a Conspicuous Material Challenge—Comprehensive Review and Future Directions. *Chemical Reviews* **2024**, *124*, 6271–6392.
(10) Yartys, V. A.; Lototskyy, M. V.; Akiba, E.; Albert, R.; Antonov, V. E.; Ares, J. R.; Baricco, M.; Bourgeois, N.; Buckley, C. E.; Bellosta von Colbe, J. M.; Crivello, J. C.; Cuevas, F.; Denys, R. V.; Dornheim, M.; Felderhoff, M.; Grant, D. M.; Hauback, B. C.; Humphries, T. D.; Jacob, I.; Jensen, T. R.; de Jongh, P. E.; Joubert, J. M.; Kuzovnikov, M. A.; Latroche, M.; Paskevicius, M.; Pasquini, L.; Popilevsky, L.; Skripnyuk, V. M.; Rabkin, E.; Sofianos, M. V.; Stuart, A.; Walker, G.; Wang, H.; Webb, C. J.; Zhu, M. Magnesium Based Materials for Hydrogen Based Energy Storage: Past, Present and Future. *Int. J. Hydrogen Energy* **2019**, *44* (15), 7809–7859.
(11) Lin, H. J.; Li, H. W.; Shao, H.; Lu, Y.; Asano, K. In Situ Measurement Technologies on Solid-State Hydrogen Storage Materials: A Review. *Mater. Today Energy* **2020**, *17*, 100463.
(12) Schneemann, A.; White, J. L.; Kang, S.; Jeong, S.; Wan, L. F.; Cho, E. S.; Heo, T. W.; Prendergast, D.; Urban, J. J.; Wood, B. C.; Allendorf, M. D.; Stavila, V. Nanostructured Metal Hydrides for Hydrogen Storage. *Chem. Rev.* **2018**, *118*, 10775–10839.
(13) Spatz, P.; Aebischer, H. A.; Krozer, A.; Schlapbach, L. The Diffusion of H in Mg and the Nucleation and Growth of MgH_2 In Thin Films. *Zeitschrift fur Physikalische Chemie* **1993**, *181*, 393.
(14) Lyu, J.; Kudiiarov, V.; Lider, A. Experimentally Observed Nucleation and Growth Behavior of Mg/MgH2 during De/Hydrogenation of MgH_2/Mg: A Review. *Materials.* **2022**, *15*, 8004.
(15) Higuchi, K.; Kajioka, H.; Toiyama, K.; Fujii, H.; Orimo, S.; Kikuchi, Y. In Situ Study of Hydriding-Dehydriding Properties in Some Pd/Mg Thin Films with Different Degree of Mg Crystallization. *J. Alloys Compd.* **1999**, *293–295* (20), 484.
(16) Mooij, L.; Dam, B. Hysteresis and the Role of Nucleation and Growth in the Hydrogenation of Mg Nanolayers. *Phys. Chem. Chem. Phys.* **2013**, *15*, 2782.
(17) Mooij, L.; Dam, B. Nucleation and Growth Mechanisms of Nano Magnesium Hydride from the Hydrogen Sorption Kinetics. *Phys. Chem. Chem. Phys.* **2013**, *15*, 11501.
(18) Bannenberg, L. J.; Schreuders, H.; Van Eijck, L.; Heringa, J. R.; Steinke, N. J.; Dalgliesh, R.; Dam, B.; Mulder, F. M.; Van Well, A. A. Impact of Nanostructuring on the Phase Behavior of Insertion Materials: The Hydrogenation Kinetics of a Magnesium Thin Film. *J. Phys. Chem. C* **2016**, *120*, 10185.
(19) Dura, J. A.; Kelly, S. T.; Kienzle, P. A.; Her, J. H.; Udovic, T. J.; Majkrzak, C. F.; Chung, C. J.; Clemens, B. M. Porous Mg Formation upon Dehydrogenation of MgH_2 Thin Films. *J. Appl. Phys.* **2011**, *109*, 093501.
(20) Hadjixenophontos, E.; Roussel, M.; Sato, T.; Weigel, A.; Stender, P.; Orimo, S.-i.; Schmitz, G. Imaging the Hydrogenation of Mg Thin Films. *Int. J. Hydrogen Energy* **2017**, *42*, 22411.
(21) Hamm, M.; Bongers, M. D.; Roddatis, V.; Dietrich, S.; Lang, K. H.; Pundt, A. In Situ Observation of Hydride Nucleation and Selective Growth in Magnesium Thin-Films with Environmental Transmission Electron Microscopy. *Int. J. Hydrogen Energy* **2019**, *44*, 32112.
(22) Uchida, H. T.; Wagner, S.; Hamm, M.; Kürschner, J.; Kirchheim, R.; Hjörvarsson, B.; Pundt, A. Absorption Kinetics and Hydride Formation in Magnesium Films: Effect of Driving Force Revisited. *Acta Mater.* **2015**, *85*, 279.
(23) Baldi, A.; Pálsson, G. K.; Gonzalez-Silveira, M.; Schreuders, H.; Slaman, M.; Rector, J. H.; Krishnan, G.; Kooi, B. J.; Walker, G. S.; Fay, M. W.; Hjörvarsson, B.; Wijngaarden, R. J.; Dam, B.; Griessen, R. Mg/Ti Multilayers: Structural and Hydrogen Absorption Properties. *Phys. Rev. B Condens Matter Mater. Phys.* **2010**, *81*, 224203.
(24) Baldi, A.; Gonzalez-Silveira, M.; Palmisano, V.; Dam, B.; Griessen, R. Destabilization of the Mg-H System through Elastic Constraints. *Phys. Rev. Lett.* **2009**, *102*, 226102.
(25) Baldi, A.; Palmisano, V.; Gonzalez-Silveira, M.; Pivak, Y.; Slaman, M.; Schreuders, H.; Dam, B.; Griessen, R. Quasifree Mg-H Thin Films. *Appl. Phys. Lett.* **2009**, *95*, 071903.
(26) Surrey, A.; Schultz, L.; Rellinghaus, B. Electron Beam Induced Dehydrogenation of MgH_2 Studied by VEELS. *Adv. Struct Chem. Imaging* **2016**, *2*, 7.
(27) Spatz, P.; Aebischer, H. A.; Krozer, A.; Schlapbach, L. The Diffusion of H in Mg and the Nucleation and Growth of MgH_2 In Thin Films. *Zeitschrift fur Physikalische Chemie* **1993**, *181*, 393.
(28) Kammerer, J. A.; Duan, X.; Neubrech, F.; Schröder, R. R.; Liu, N.; Pfannmöller, M. Stabilizing γ-MgH_2 at Nanotwins in Mechanically Constrained Nanoparticles. *Adv. Mater.* **2021**, *33*, 2008529.
(29) Karst, J.; Sterl, F.; Linnenbank, H.; Weiss, T.; Hentschel, M.; Giessen, H. Watching in Situ the Hydrogen Diffusion Dynamics in Magnesium on the Nanoscale. *Sci. Adv.* **2020**, *6*, 0056.
(30) Sterl, F.; Strohfeldt, N.; Walter, R.; Griessen, R.; Tittl, A.; Giessen, H. Magnesium as Novel Material for Active Plasmonics in the Visible Wavelength Range. *Nano Lett.* **2015**, *15*, 7949.
(31) Westerwaal, R. J.; Borgschulte, A.; Lohstroh, W.; Dam, B.; Kooi, B.; ten Brink, G.; Hopstaken, M. J. P.; Notten, P. H. L. The Growth-Induced Microstructural Origin of the Optical Black State of Mg2NiHx Thin Films. *J. Alloys Compd.* **2006**, *416*, 2.